Rogue waves with rational profiles in unstable condensate and its solitonic model.

D. Agafontsev[1,2] and A. Gelash[2,3].

[1] - *P.P. Shirshov Institute of Oceanology of RAS, Moscow, Russia.*
[2] - *Skolkovo Institute of Science and Technology, Moscow, Russia.*
[3] - *Institute of Automation and Electrometry of SB RAS, Novosibirsk, Russia.*

XIX Session of the Russian Academy of Sciences Council on nonlinear dynamics, 14-15 December 2020.

Introduction.

In this work we consider two systems, both within the focusing 1D Nonlinear Schrodinger Equation (1D-NLSE),

$$i\psi_t + \psi_{xx} + |\psi|^2 \psi = 0.$$

System 1: modulational instability (MI) of the condensate at its long-time statistically stationary state.

If we start from the condensate solution **ψ=1** perturbed by small initial noise **ε(x)**, which is considered to be space-homogeneous,

$$\psi|_{t=0} = 1 + \varepsilon(x),$$

then after a long evolution we will come to the so-called statistically stationary state – the state in which the basic statistical functions (the moments, the wave-action spectrum, the PDF of intensity, etc), averaged over noise realizations, are independent of time.
[D.S. Agafontsev, V.E. Zakharov, Nonlinearity 28, 2791 (2015)]

System 2: soliton gas modelling the system 1. It turns out that there exists specific soliton gas, that accurately models the statistically stationary state of the MI.
[A. Gelash, D. Agafontsev, V. Zakharov, G. El, S. Randoux and P. Suret, Phys. Rev. Lett. 123, 234102 (2019)]

Introduction.

This soliton gas has the following properties:

1) Soliton IST eigenvalues are located on the imaginary axis and given by the Bohr-Sommerfeld quantization rule,

$$\lambda_j = i\sqrt{1-\left(\frac{j-1/2}{M}\right)^2}$$

Here **M** is the number of solitons and **j = 1,…,M**. Soliton amplitudes and velocities are recovered from the eigenvalues as $\mathbf{a_j = 2\ Im\ \lambda_j}$ and $\mathbf{v_j = 2\ Re\ \lambda_j}$, so that all soliton velocities are zero and they form a bound state, and the maximum soliton amplitude is slightly smaller than **2**.

2) Soliton positions are random with uniform distribution in a narrow interval at the coordinates origin (formally, we can place all solitons in one point, $\mathbf{x_j=0}$, but in this case our multi-soliton solution will be symmetric and we would like to avoid this symmetry from one hand, and keep the soliton density high from the other).

3) By analogy with an incoherent state of a linear system, soliton phases are random with uniform distribution in the interval $\mathbf{\theta_j \in [0, 2\pi)}$.

Introduction.

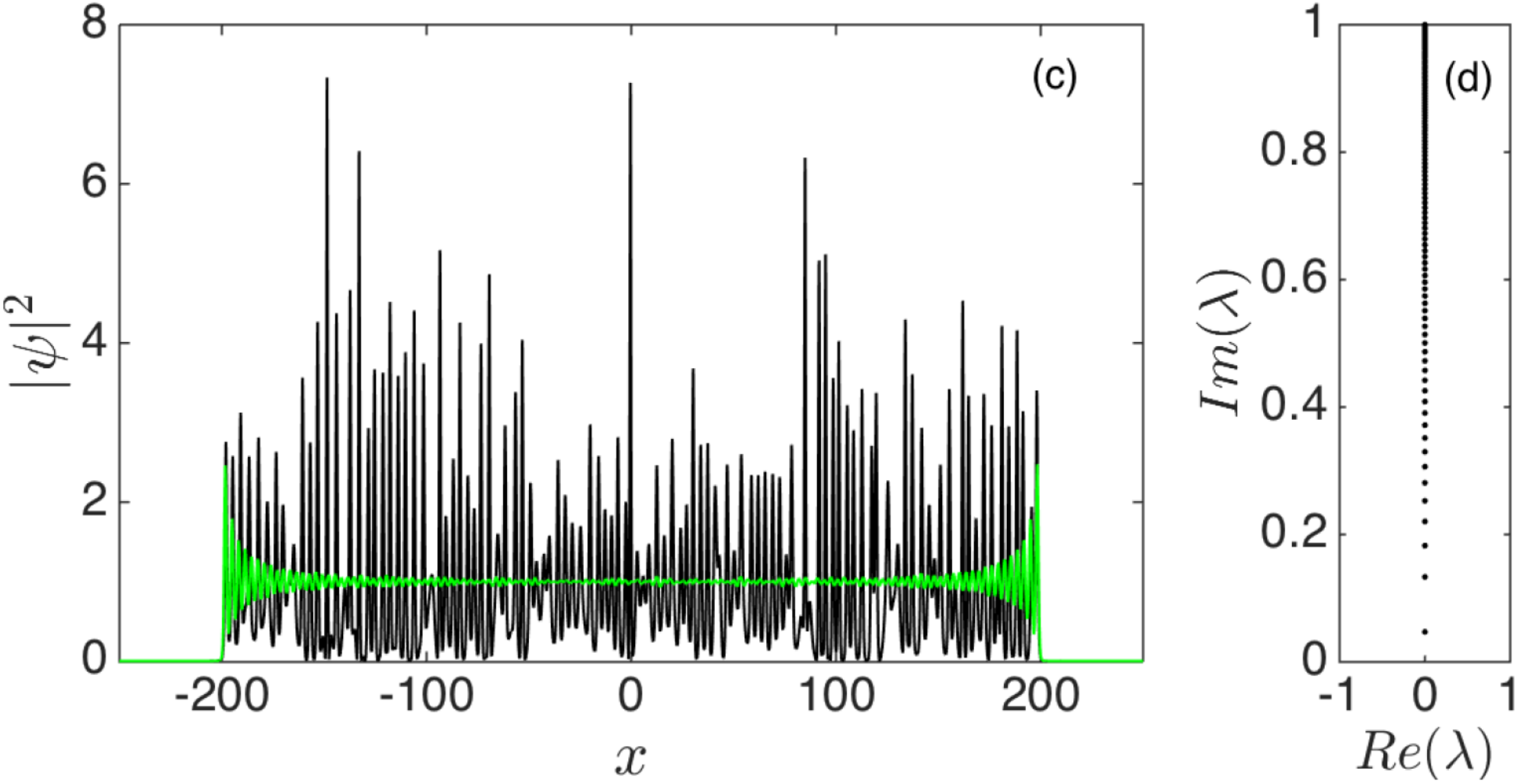

This soliton gas is practically uniform in space (in the statistical sense) in an extended region of about 70% of its characteristic length. Here the green line shows the intensity averaged over ensemble and time, **$I(x) = \langle|\psi(x,t)|^2\rangle$**; the number of solitons is **128**.

Introduction.

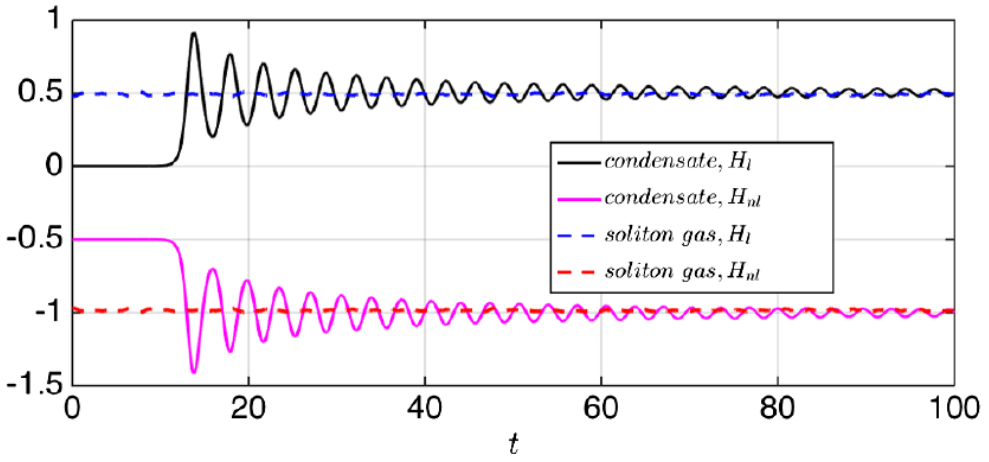

FIG. 3. Time evolution of the ensemble-averaged kinetic $\langle H_l(t)\rangle$ and potential $\langle H_{nl}(t)\rangle$ energies for the noise-induced MI (black and magenta solid lines) and random phase SG (blue and red dashed lines).

The soliton gas is in the statistically stationary state from its creation, and its statistical characteristics match those of the noise-induced MI at its long-time statistically stationary state.

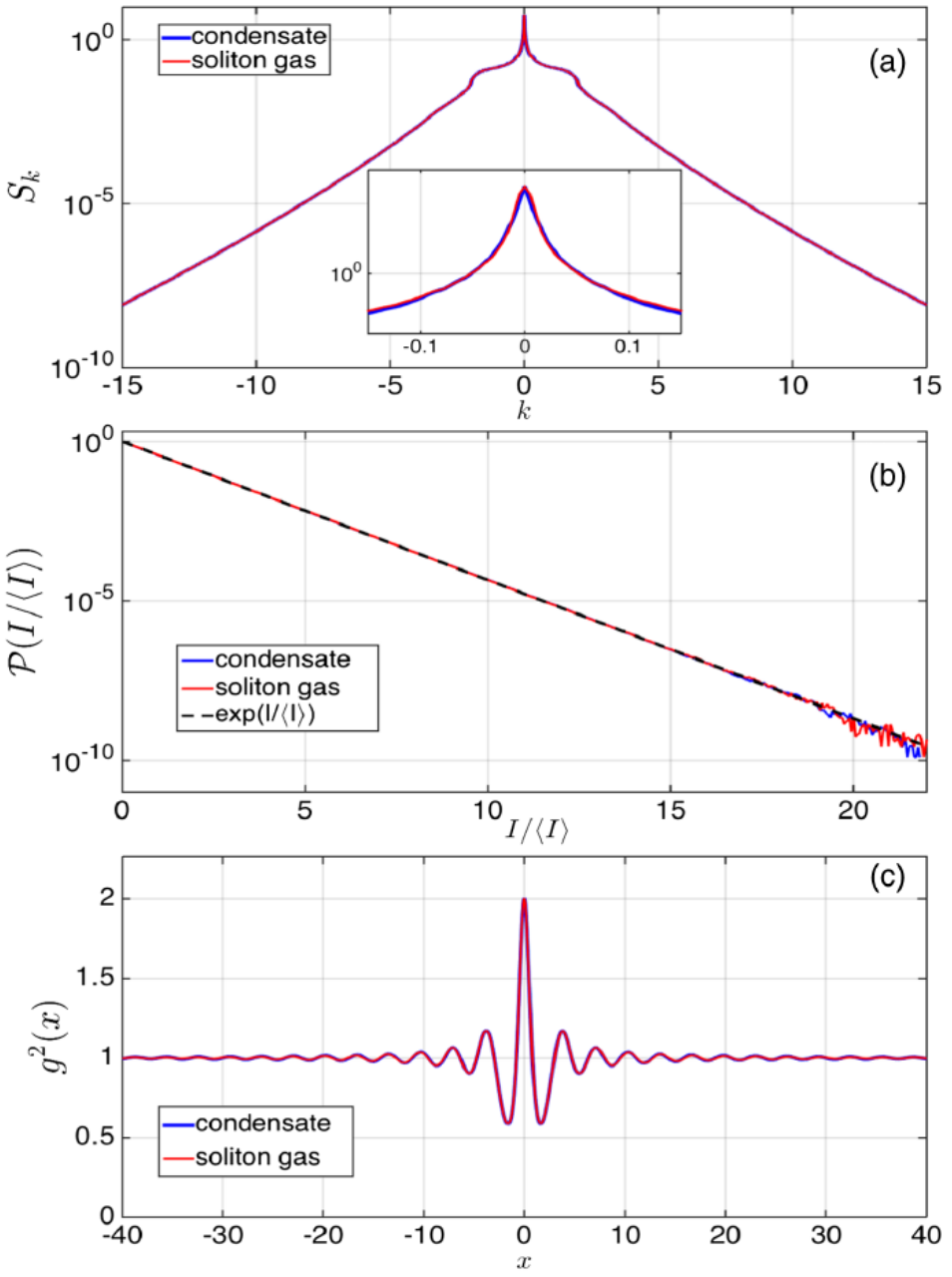

Introduction.

The main question we are trying to answer in this study is:

OK, the two systems show identical statistics. Then, maybe, the rogue waves (RWs) for these two systems behave identically?

If so, then, since for the soliton gas all rogue waves are interaction of solitons, we can draw a hypothesis that for the asymptotic stationary state of the MI (and, possibly, for other strongly nonlinear wavefields) the main mechanism of RW formation is interaction of solitons.

In the following, we will compare RWs for the two systems with rational breather solutions (e.g., Peregrine breather). This means that, effectively, we consider solutions of the 1D-NLSE for three different types of boundary conditions: (1) periodic boundary for the MI, (2) vanishing border conditions for multi-soliton solutions and (3) constant border conditions for rational breathers. For instance, formally our MI case corresponds to finite-band scattering data. However, the characteristic widths of the structures (RWs, solitons, rational breathers) are small compared to the sizes of the studied wavefields, so that the eigenvalue bands are very narrow and we neglect their difference from solitons. Effectively, we assume that formation of a RW, as a local phenomenon, represents a similar process for all three cases of border conditions.

Numerical methods.

We create ensembles of **1000** realizations for each type of initial conditions:
(1) the condensate perturbed by small initial noise (realizations differ by random noise),
(2) soliton gas containing **128** solitons modelling the stationary state of the MI (realizations differ by random soliton positions and phases).

Then we simulate their time evolution using the Runge-Kutta 4^{th} order method on adaptive grid combined with Fourier interpolation between the grids. This method conserves the first 10 invariants with accuracy better than 10^{-6}.

For each realization of initial conditions, we collect one largest RW that emerged in the course of the evolution. For the MI case, the time window in which we collect the RWs is shifted to large times, when the system is sufficiently close to the statistically stationary state.

In the end, we compare **1000** largest RWs for the MI case with **1000** largest RWs for the soliton gas modelling the MI.

Such a comparison has a significant drawback, as we do not compare the “common” RWs for the two systems, which may have different dynamical and statistical properties. But our main idea here is that, if the cohorts of the largest RWs will show the same properties, then we may suggest that the “common” RWs have the same properties too.

Numerical methods.

In the following, we will fit the collected RWs with rational breather solutions (RBS) – the Peregrine breather (RBS of the first order – or RBS1) and the RBS of the second order (RBS2). The Peregrine breather (RBS1) read as

$$\psi_p^{(1)}(x,t) = e^{it}\left[1 - \frac{4(1+2it)}{1+2x^2+4t^2}\right].$$

The RBS2 it too cumbersome, and can be found in *[N. Akhmediev, A. Ankiewicz and J. M. Soto-Crespo, Phys. Rev. E 80, 026601 (2009)]*.

Results.

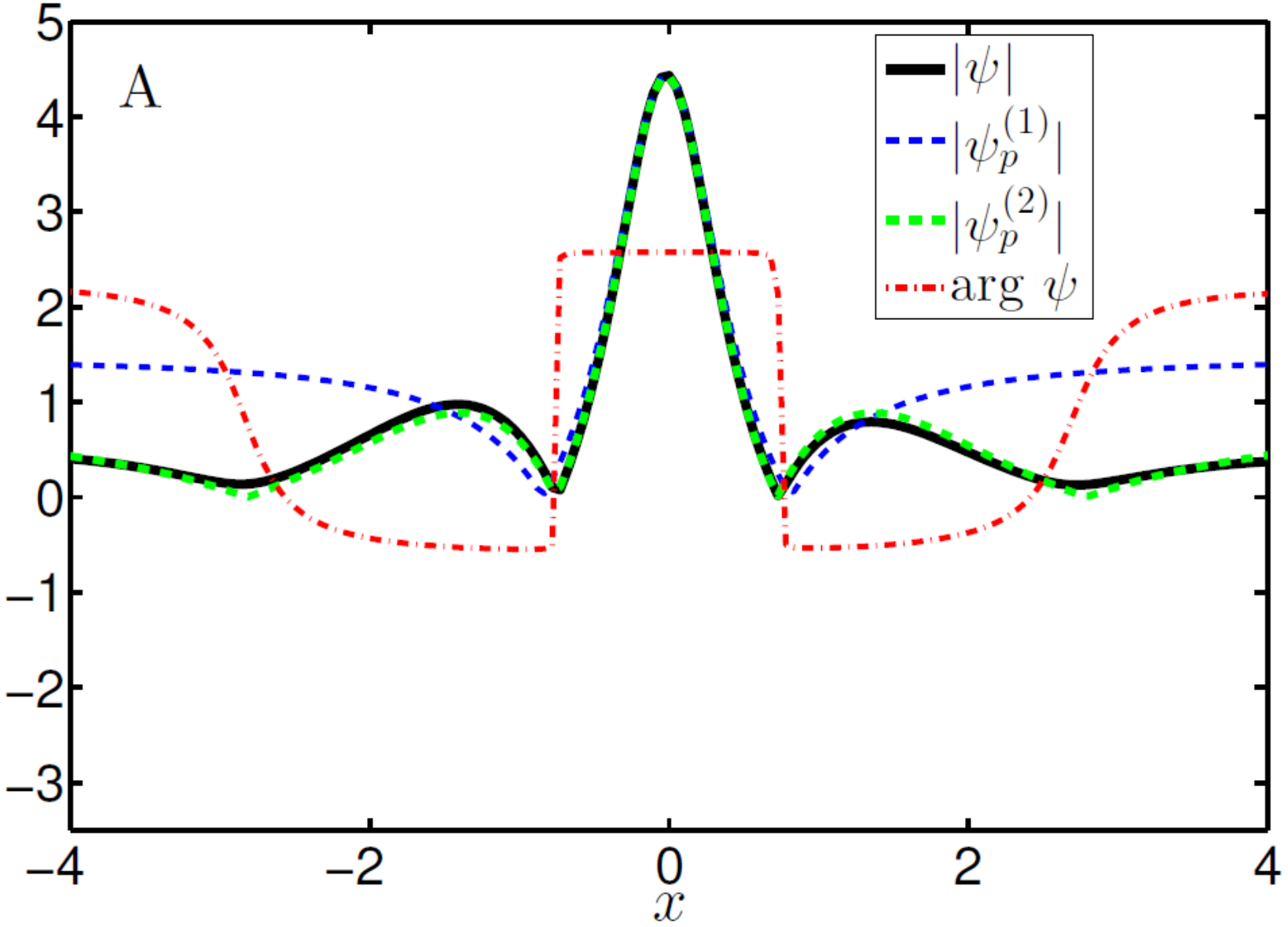

One of the 10 largest collected RWs, the soliton gas case.

Results.

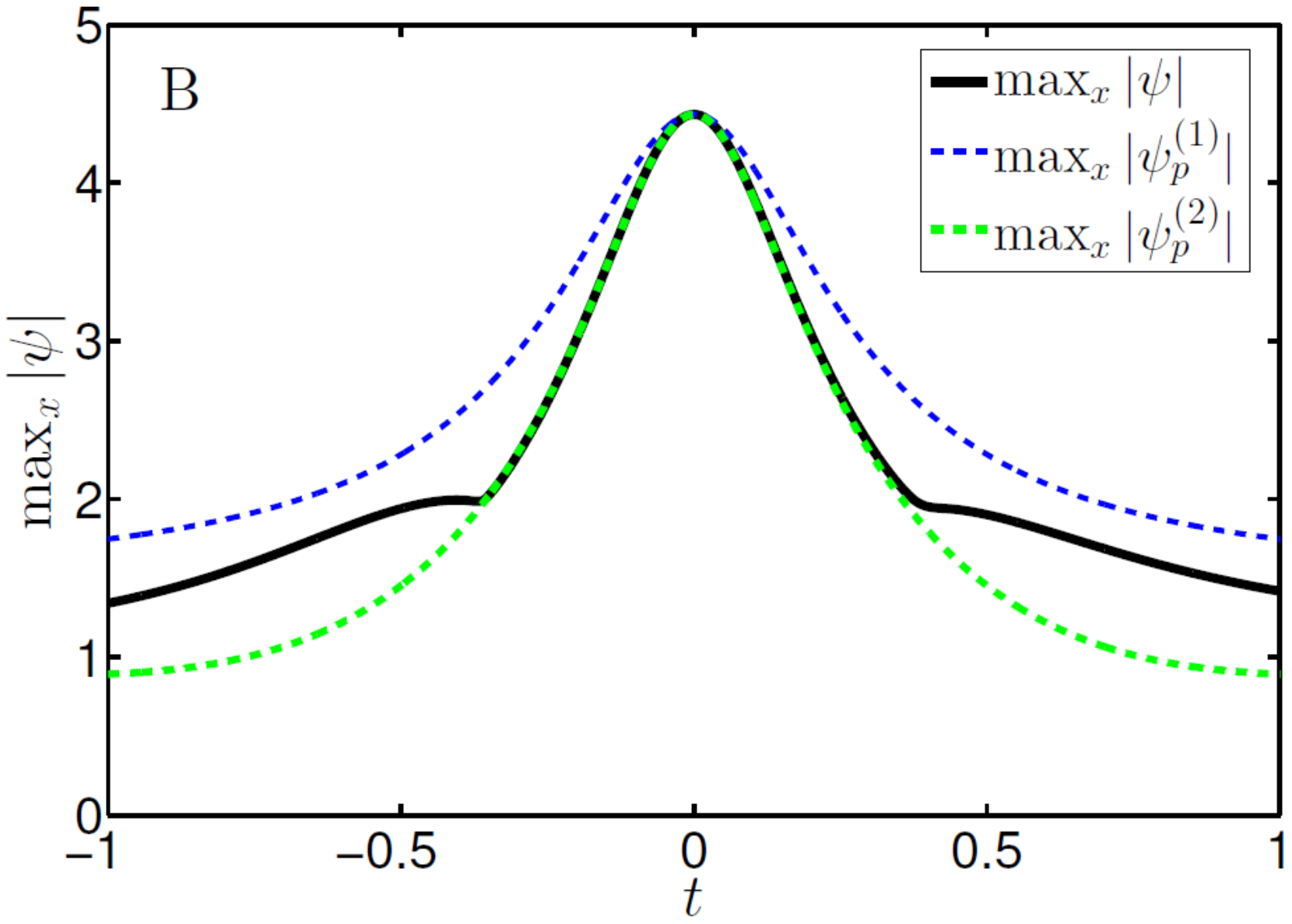

One of the 10 largest collected RWs, the soliton gas case.

Results.

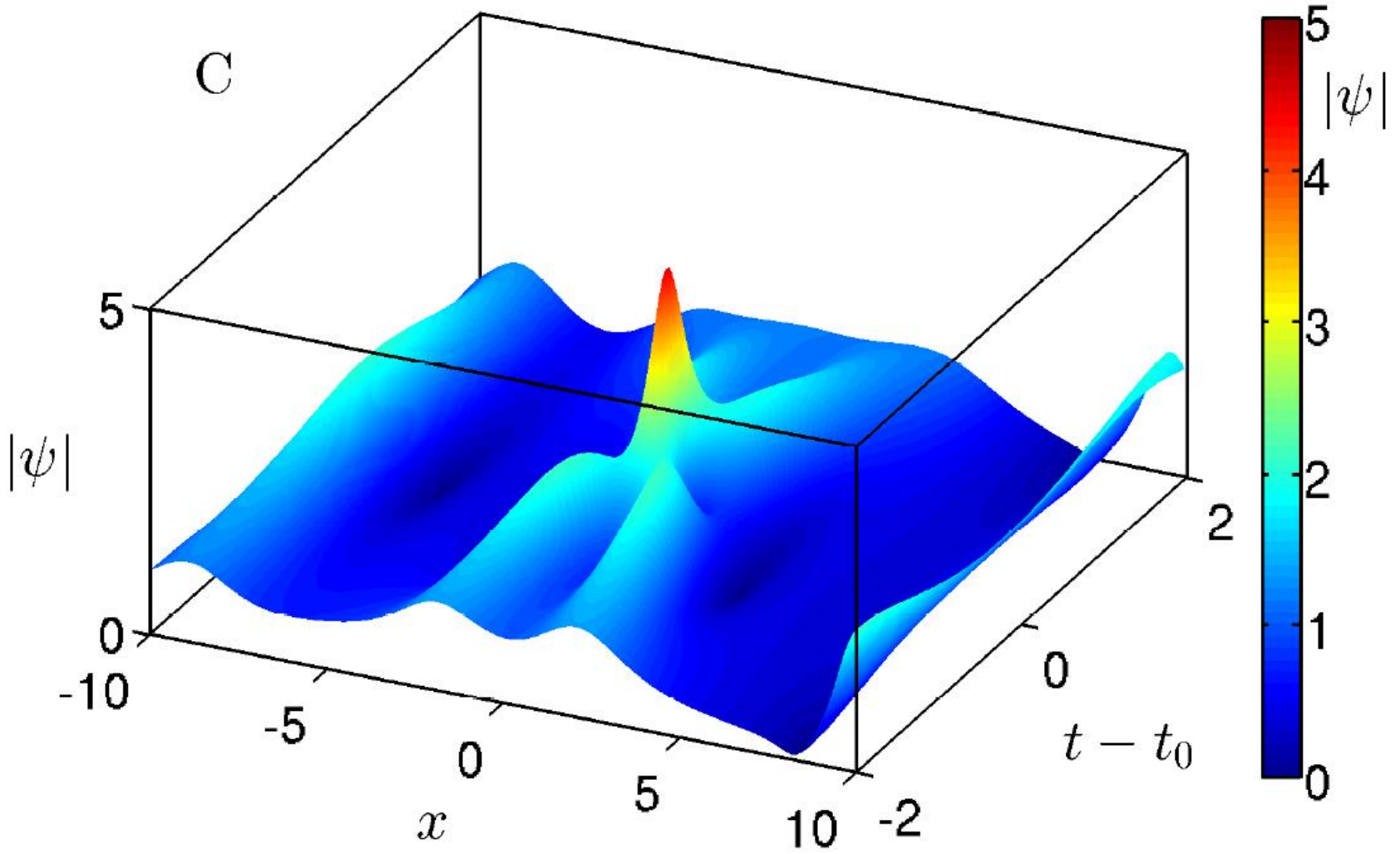

One of the 10 largest collected RWs, the soliton gas case.

Results.

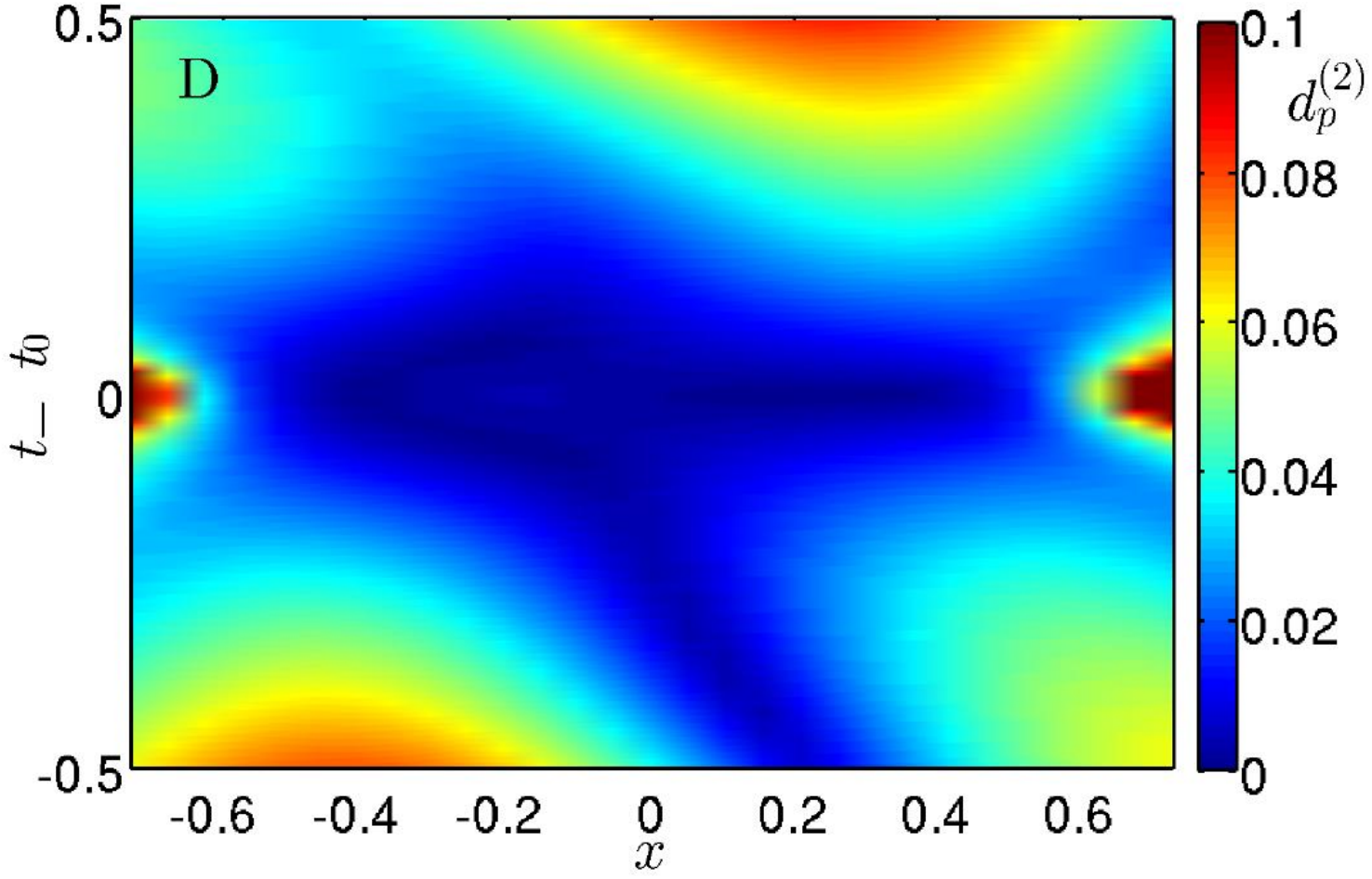

One of the 10 largest collected RWs, the soliton gas case.

We will also measure the deviation between a RW and its approximation with a RBS in the (x,t)-plane as

$$d_p^{(1,2)}(x,t) = \frac{|\psi - \psi_p^{(1,2)}|}{|\psi|}.$$

Results.

Automation of the process: as an integral measure reflecting the deviation between a RW and a RBS, one can consider the quantity

$$\mathcal{D}_p^{(1,2)} = \left[\frac{\int_{x\in\Omega}\int_{t_0-\Delta T}^{t_0+\Delta T} |\psi - \psi_p^{(1,2)}|^2 \, dxdt}{\int_{x\in\Omega}\int_{t_0-\Delta T}^{t_0+\Delta T} |\psi|^2 \, dxdt}\right]^{1/2}.$$

Here we choose the region of integration over time **$t \in [t_0-\Delta T, t_0+\Delta T]$** from the condition that at t = **$t_0 \pm \Delta T$** the RBS2 fit halves its maximum amplitude. For the previous example, **$D_p^{(2)} \approx 0.02$**.

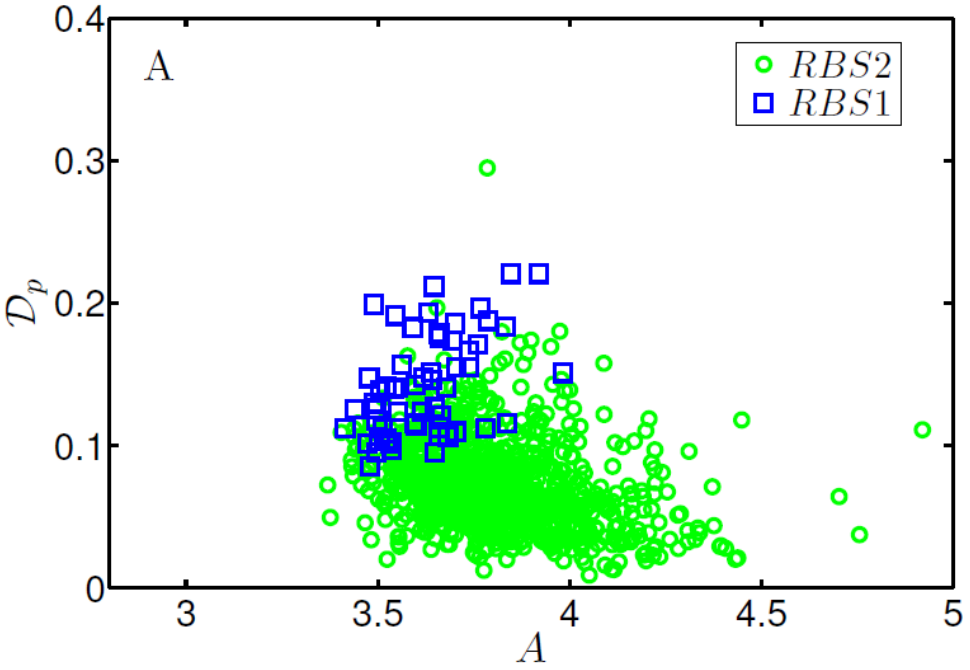

Soliton gas

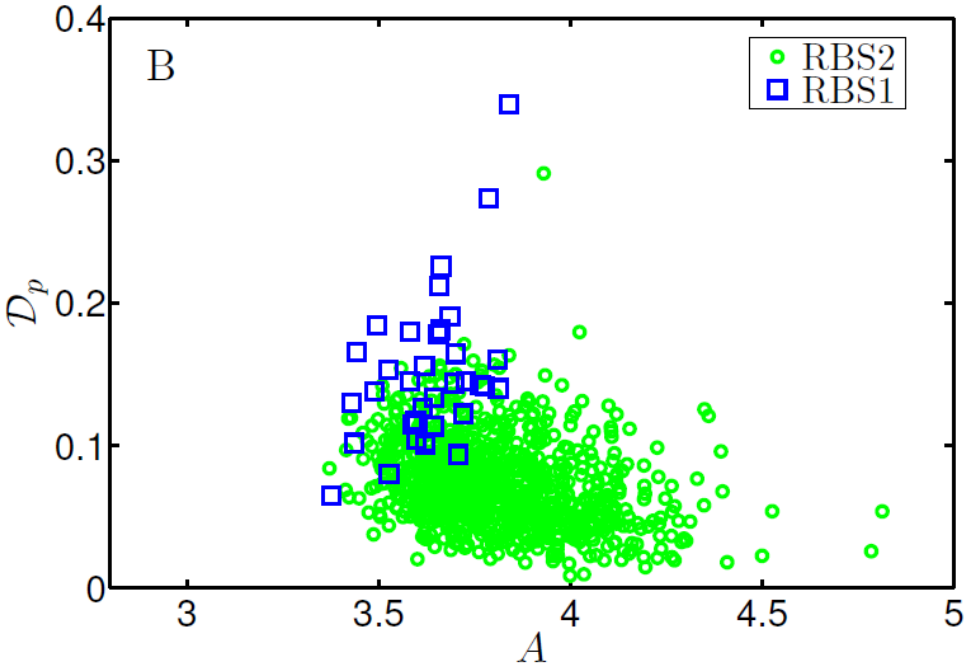

MI

Results.

According to our observations, the value of the deviation $\mathbf{D_p}$ below **0.05** typically means that the corresponding RW is very well approximated with the RBS; for $\mathbf{0.05 \leq D_p \leq 0.1}$ the approximation is satisfactory, and for $\mathbf{0.1 \leq D_p}$ – poor.

We see from the figures, that approximation with the RBS1 is satisfactory at best.

For the RBS2 we have a completely different picture:

(1) for the soliton gas case, of 943 RWs better approximated with the RBS2, 768 RWs show deviations from the RBS2 below 0.1 and 220 among them - below 0.05.

(2) for the MI case, of 964 RWs better approximated with the RBS2, 792 have deviations below 0.1 and 215 - below 0.05.

Moreover, the larger the maximum amplitude, the better (typically) the correspondence between the RWs and the RBS2.

Results.

Statistical properties: the collected RWs turn out to be identically distributed by their maximal amplitude and deviation from the RBS2.

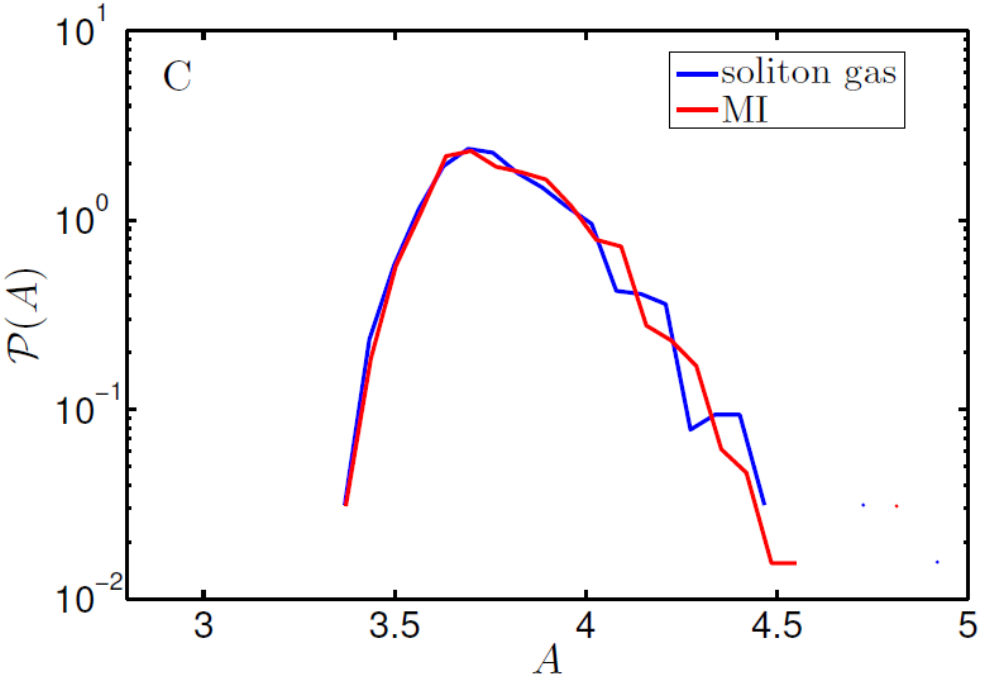

Soliton gas

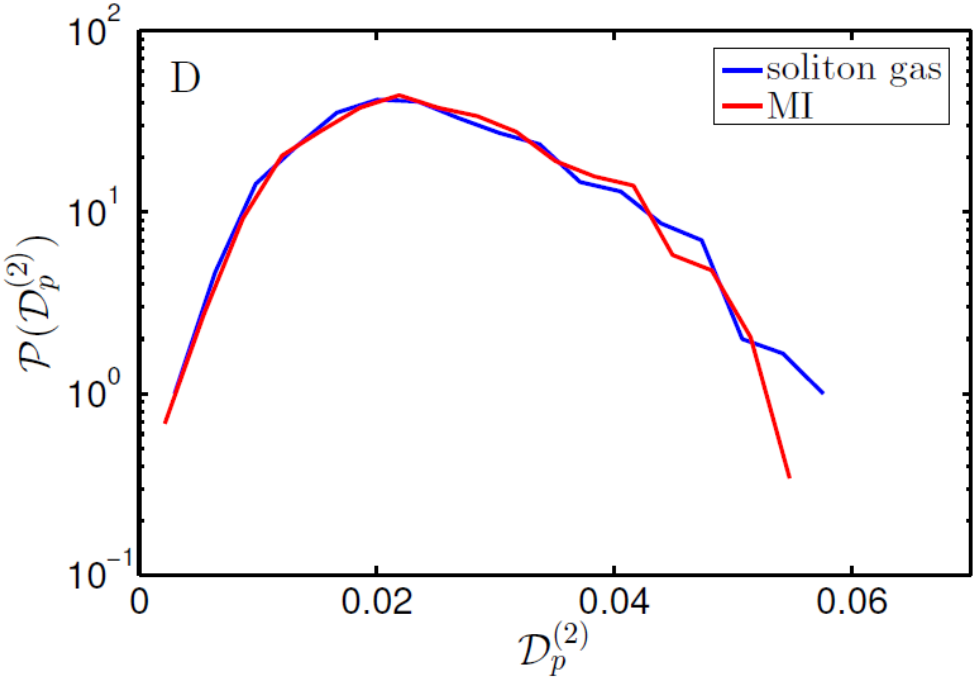

MI

Conclusion 1: the collected RWs for the two systems have practically identical dynamical (resemblance with the RBS2) and statistical properties, and we may suggest that the main mechanism of RW formation for the MI case (and possibly for other strongly nonlinear wavefields) is interaction of solitons.

Discussion.

Back in *[A.A. Gelash and D.S. Agafontsev, Phys. Rev. E 98, 042210 (2018)]* we demonstrated examples of two- and three-soliton collisions that were very well approximated by the RBS1 and the RBS2 respectively. The solitons in these examples had non-zero velocities. We now modify the three-soliton example for zero velocities; the solitons have amplitudes **1**, **1.5** and **2**, zero phases, $\boldsymbol{\theta_j=0}$, and zero positions, $\boldsymbol{x_j=0}$.

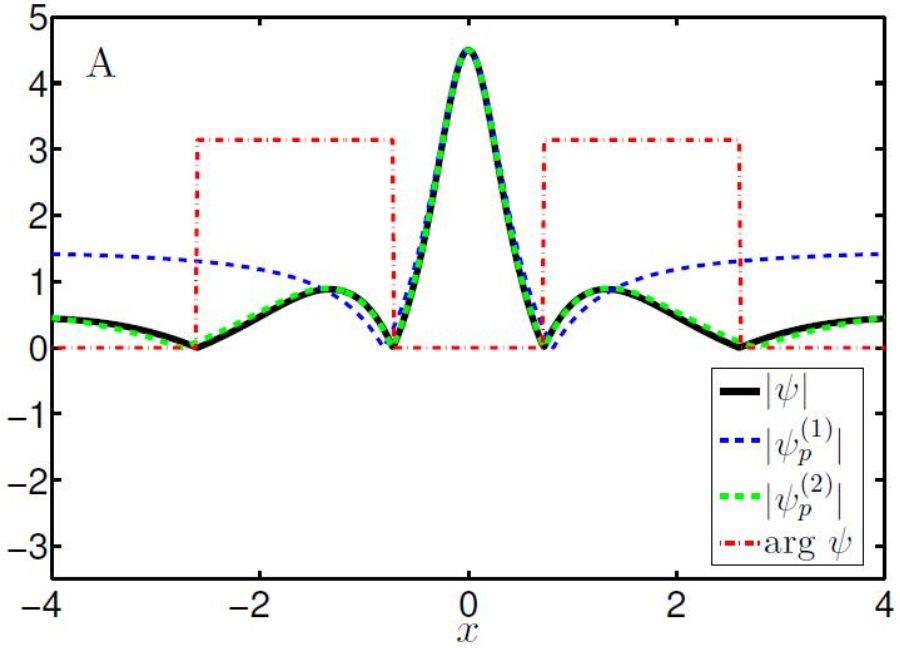

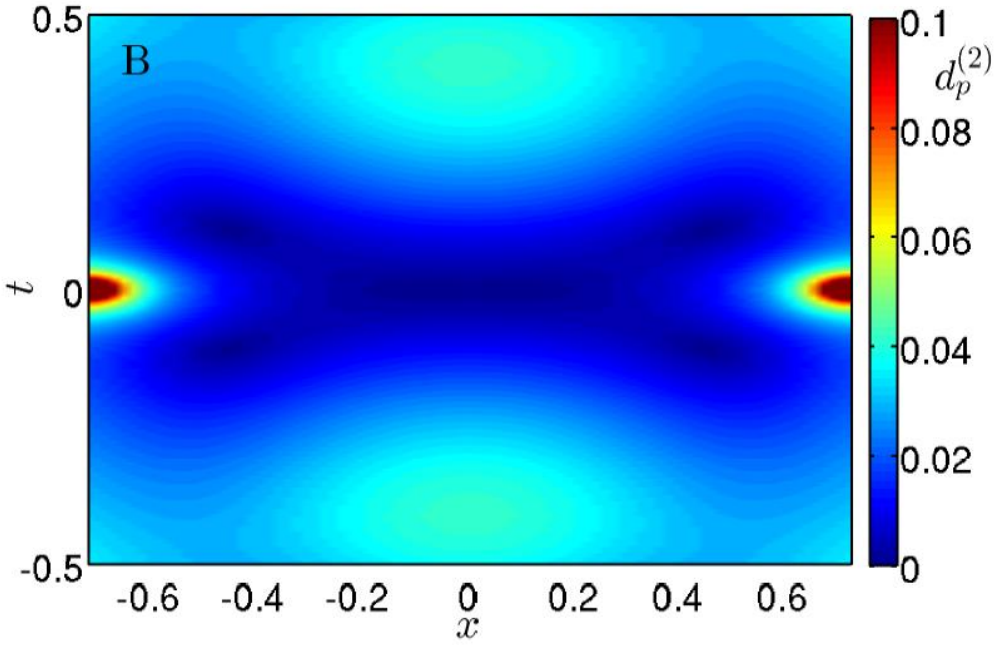

The deviation from the RBS2 fit is $\boldsymbol{D_p^{(2)} \approx 0.016}$.

Discussion.

To analyze how often the phase-synchronized interactions of two and three solitons of various amplitudes may lead to such quasi-rational profiles, we have created 20 two-soliton and 20 three-soliton interactions with solitons of random amplitudes, zero velocities, zero space positions parameters and phases.

For the two-soliton interactions, the minimum deviations from the RBS1 and the RBS2 turned out to be $\mathbf{D_p^{(1)} \approx 0.077}$ and $\mathbf{D_p^{(2)} \approx 0.061}$.

For the three-soliton case, the minimum deviations were $\mathbf{D_p^{(1)} \approx 0.18}$ and $\mathbf{D_p^{(2)} \approx 0.003}$ (!!!) and the average ones -- $\mathbf{\langle D_p^{(1)} \rangle \approx 0.23}$ and $\mathbf{\langle D_p^{(2)} \rangle \approx 0.022}$; the maximum deviation from the RBS2 equaled to $\mathbf{D_p^{(2)} \approx 0.03}$, that is still very good for comparison with the RBS2.

Conclusion 2: quasi-rational profiles very similar to that of the RBS2 appear already for three-soliton interactions, provided that the solitons are properly synchronized (that is, have coinciding positions and phases).

The question now is, if we limit ourselves with the solitonic content of the wavefield only, then how the RWs appear?

We can think of two scenarios: “collective” (then synchronization of all the solitons is necessary) and “local” (then synchronization of only a few is required).

Soliton models of typical RW solutions.

Then, how a “collective” scenario may look like? – We have some preliminary results here!

The typical RW solutions have the following (IST) spectral portraits:

(1) Peregrine solution (RBS1) – branch cut from **[0, i]** plus one soliton with $\boldsymbol{\lambda = i}$;
(2) RBS2 – branch cut from **[0, i]** plus two solitons with $\boldsymbol{\lambda_{1,2} = i}$;
(3) Kuznetsov-Ma solution – branch cut from **[0, i]** plus one soliton with $\boldsymbol{\lambda = i*\eta}$, $\boldsymbol{\eta>1}$;
(4) Akhmediev solution – branch cut from **[0, i]** plus one soliton with $\boldsymbol{\lambda = i*\eta}$, $\boldsymbol{0<\eta<1}$.

Here the branch cut is the manifestation of the constant background (the condensate). And as Andrey Gelash recently told in one of our seminars, we know how to model the condensate with the soliton gas.

In the following picture, all solitons have IST eigenvalues according to the Bohr-Sommerfeld rule, zero positions $\boldsymbol{x_j = 0}$ and phases **[0, π, 0, π, …]**.

When, what happens if we change the branch cut by our solitonic model of the condensate?

The following results were obtained in collaboration with Pierre Suret and Stephane Randoux from Lille University, France.

Soliton models of typical RW solutions.

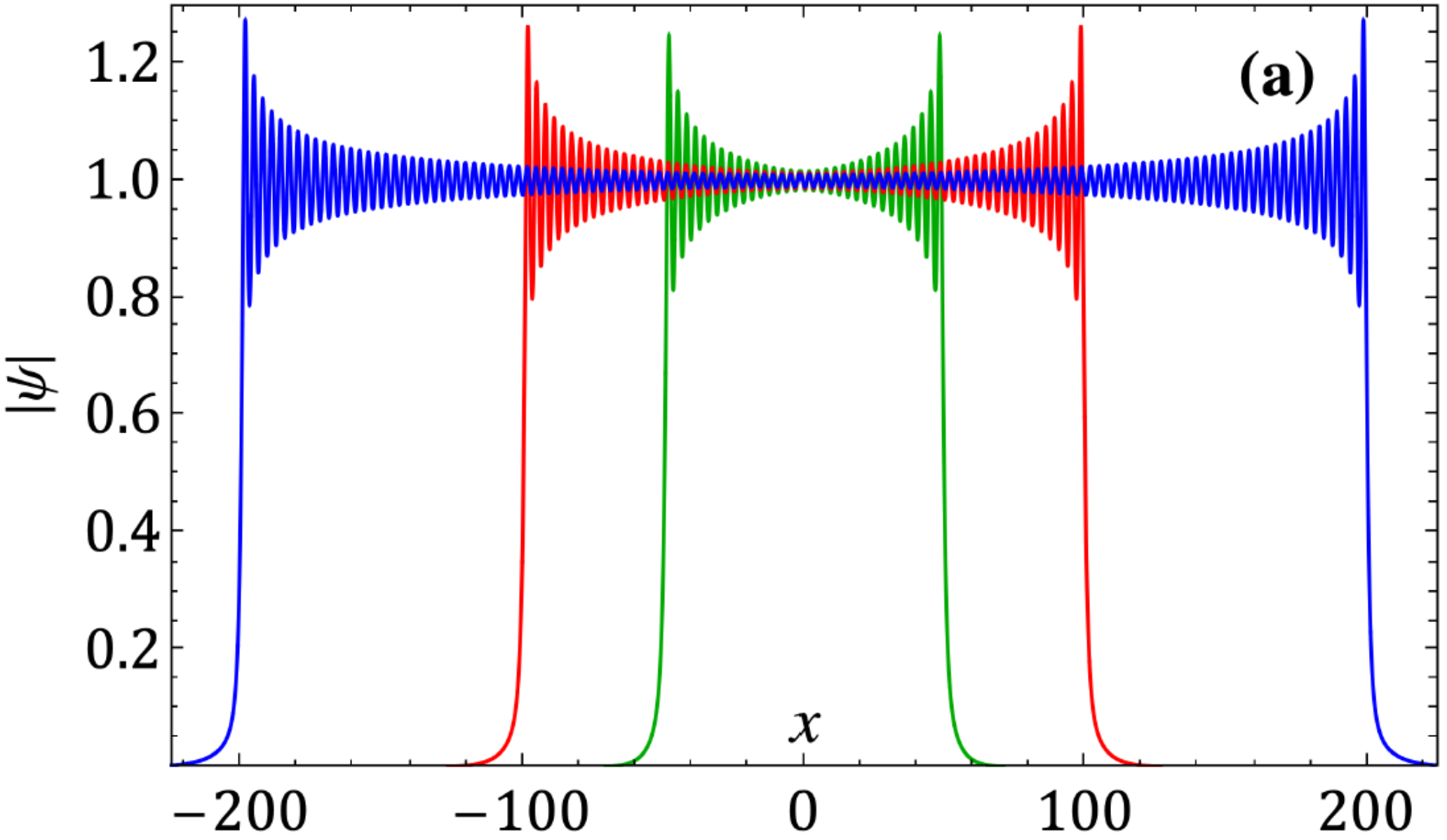

Green – 32-SS, red – 64-SS, blue – 128-SS.

Soliton models of typical RW solutions.

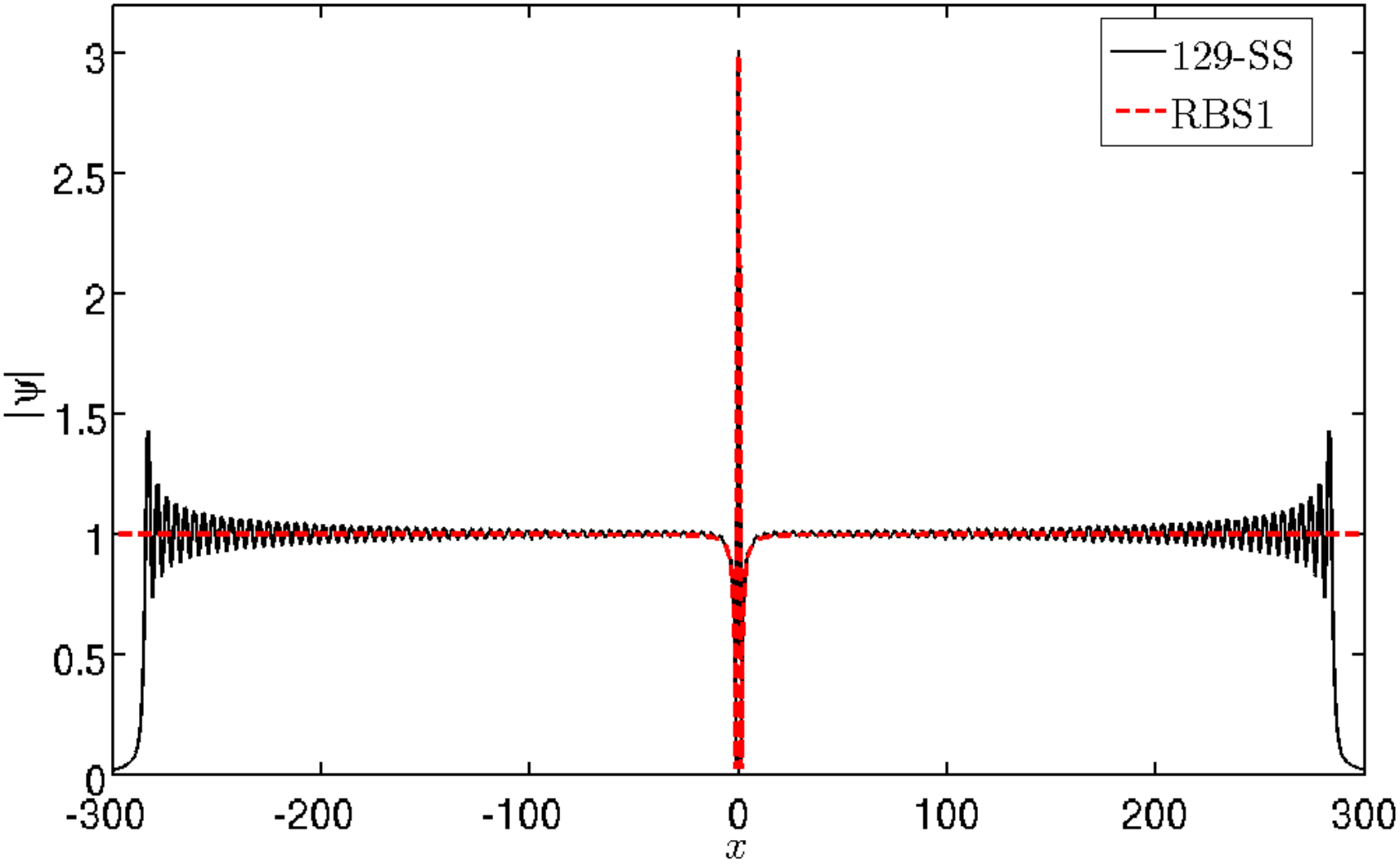

Peregrine breather modelled with 129-SS: the additional soliton has IST eigenvalue **λ = i*1.01** and phase **θ = π**; all positions are zero.

Soliton models of typical RW solutions.

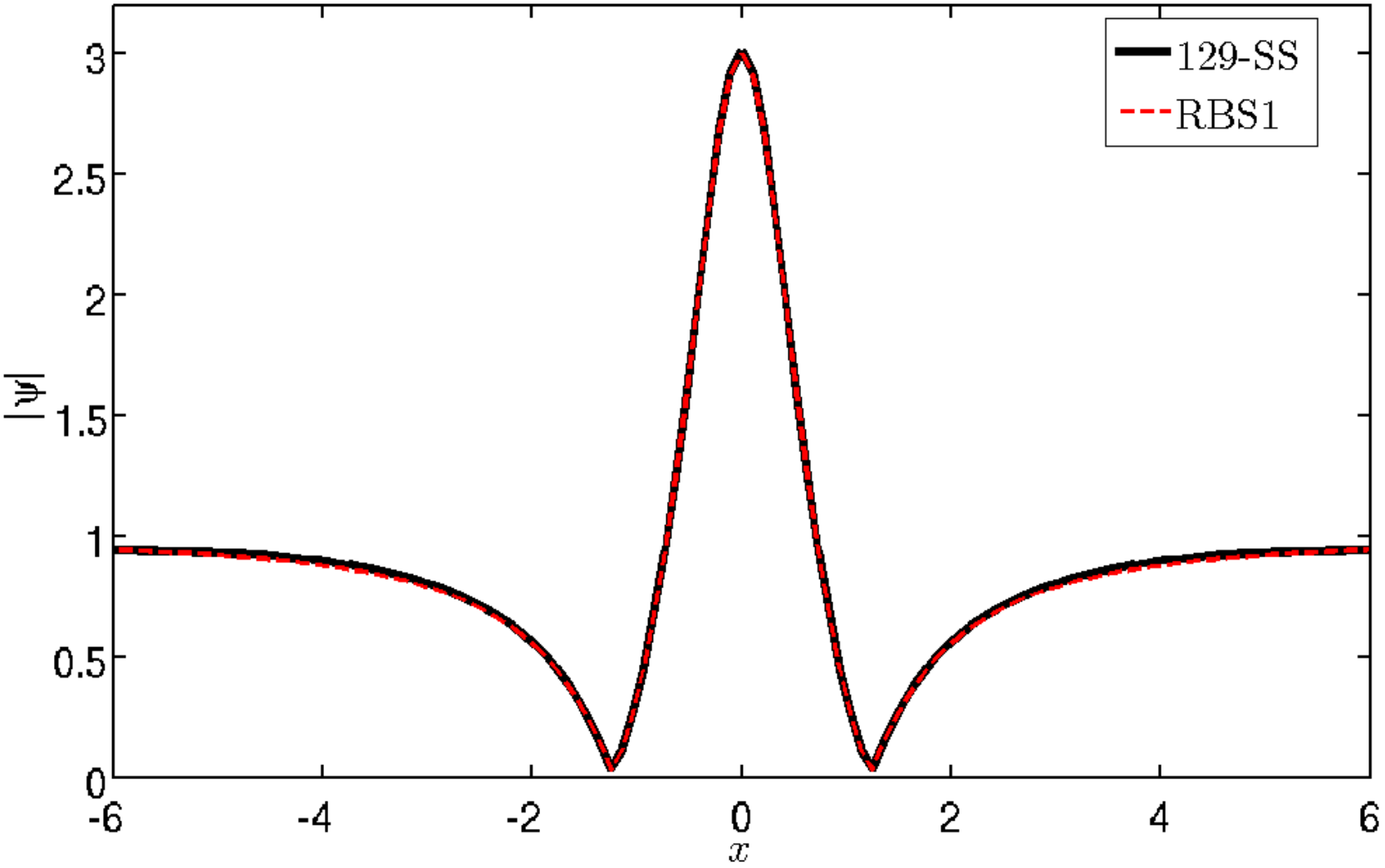

Peregrine breather modelled with 129-SS: the additional soliton has IST eigenvalue **λ = i*1.01** and phase **θ = π**; all positions are zero.

Soliton models of typical RW solutions.

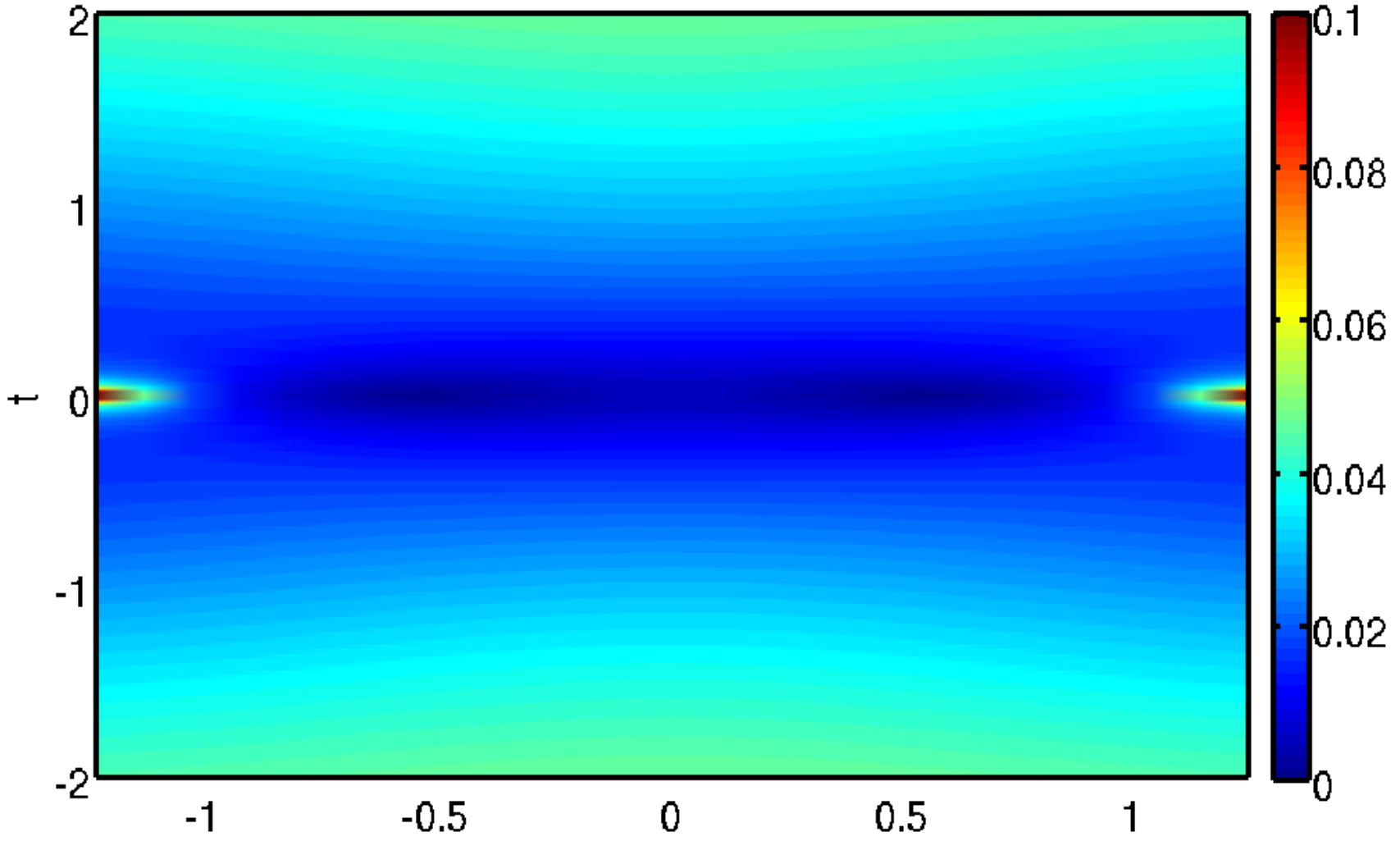

Peregrine breather modelled with 129-SS: the additional soliton has IST eigenvalue **λ = i*1.01** and phase **θ = π**; all positions are zero.

Soliton models of typical RW solutions.

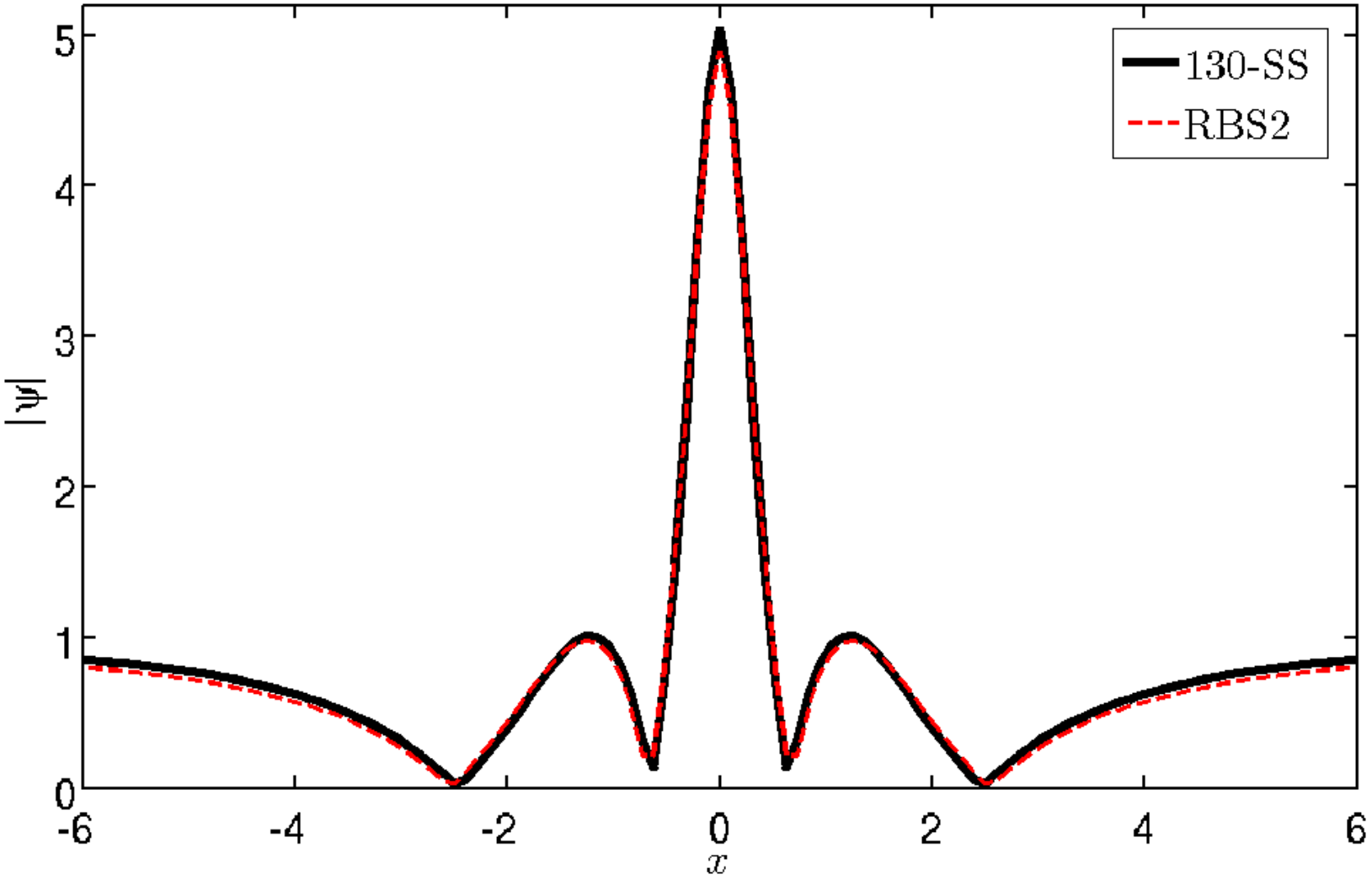

RBS2 modelled with 130-SS: the additional solitons have IST eigenvalues $\lambda_1 = i*1.01$, $\lambda_2 = i*1.02$ and phases $\theta_1 = \theta_2 = \pi$; all positions are zero.

Soliton models of typical RW solutions.

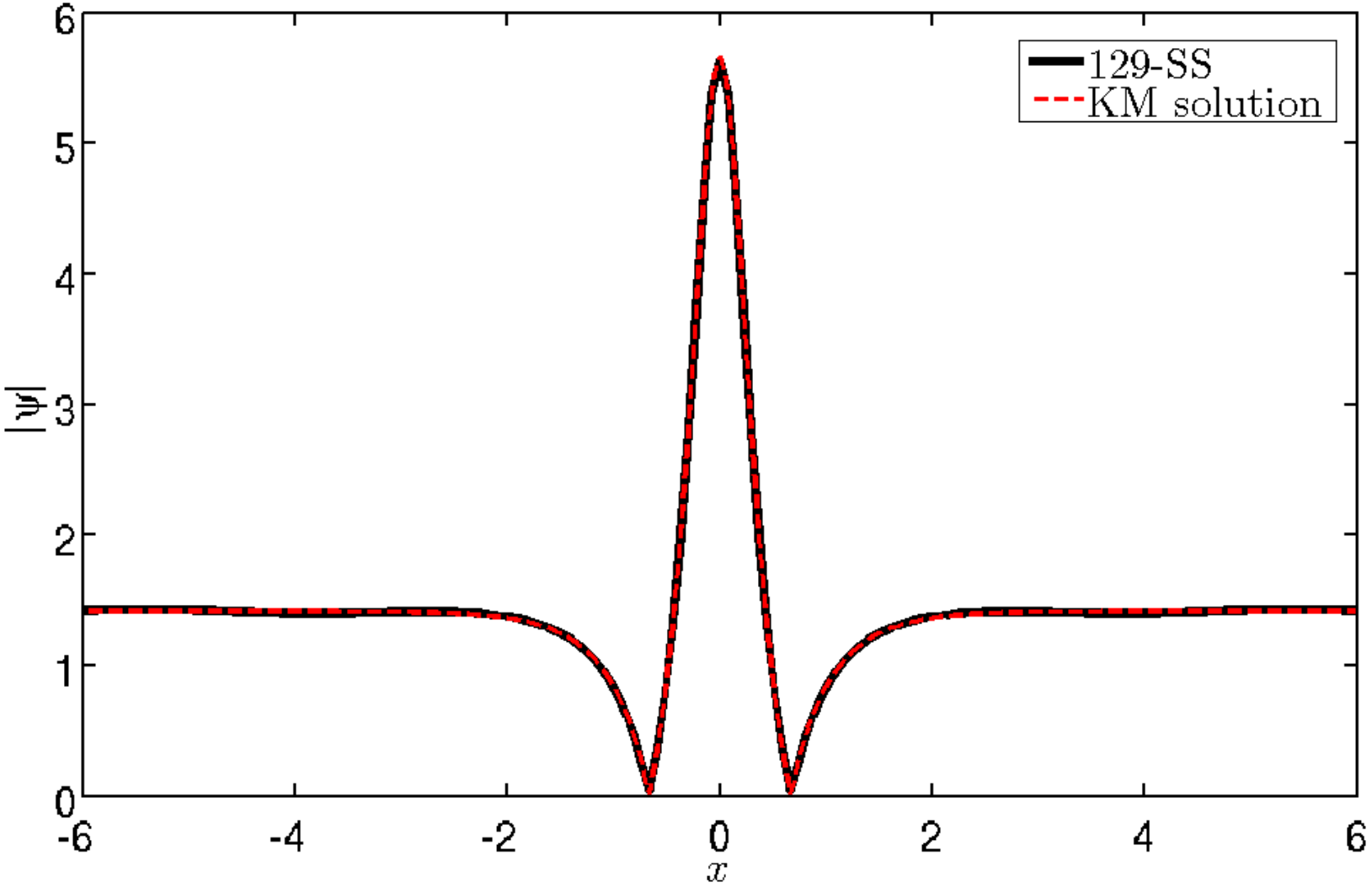

Kuznetsov-Ma solution modelled with 129-SS: the additional soliton has IST eigenvalue **λ = i*1.5** and phase **θ = π**; all positions are zero.

Soliton models of typical RW solutions.

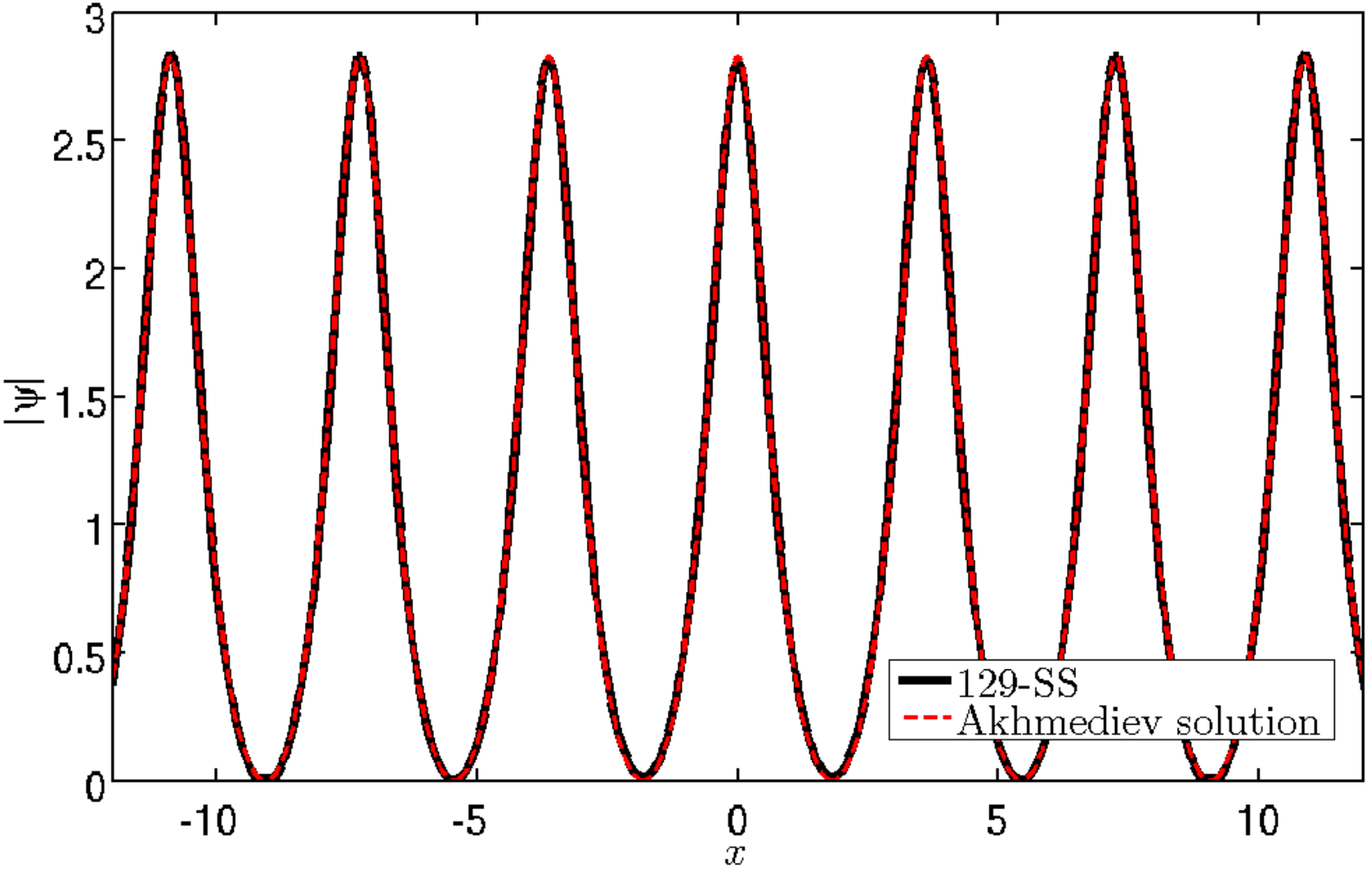

Akhmediev solution modelled with 129-SS: the additional soliton has IST eigenvalue **λ = i*0.5** and phase **θ = π**; all positions are zero.

Soliton models of typical RW solutions.

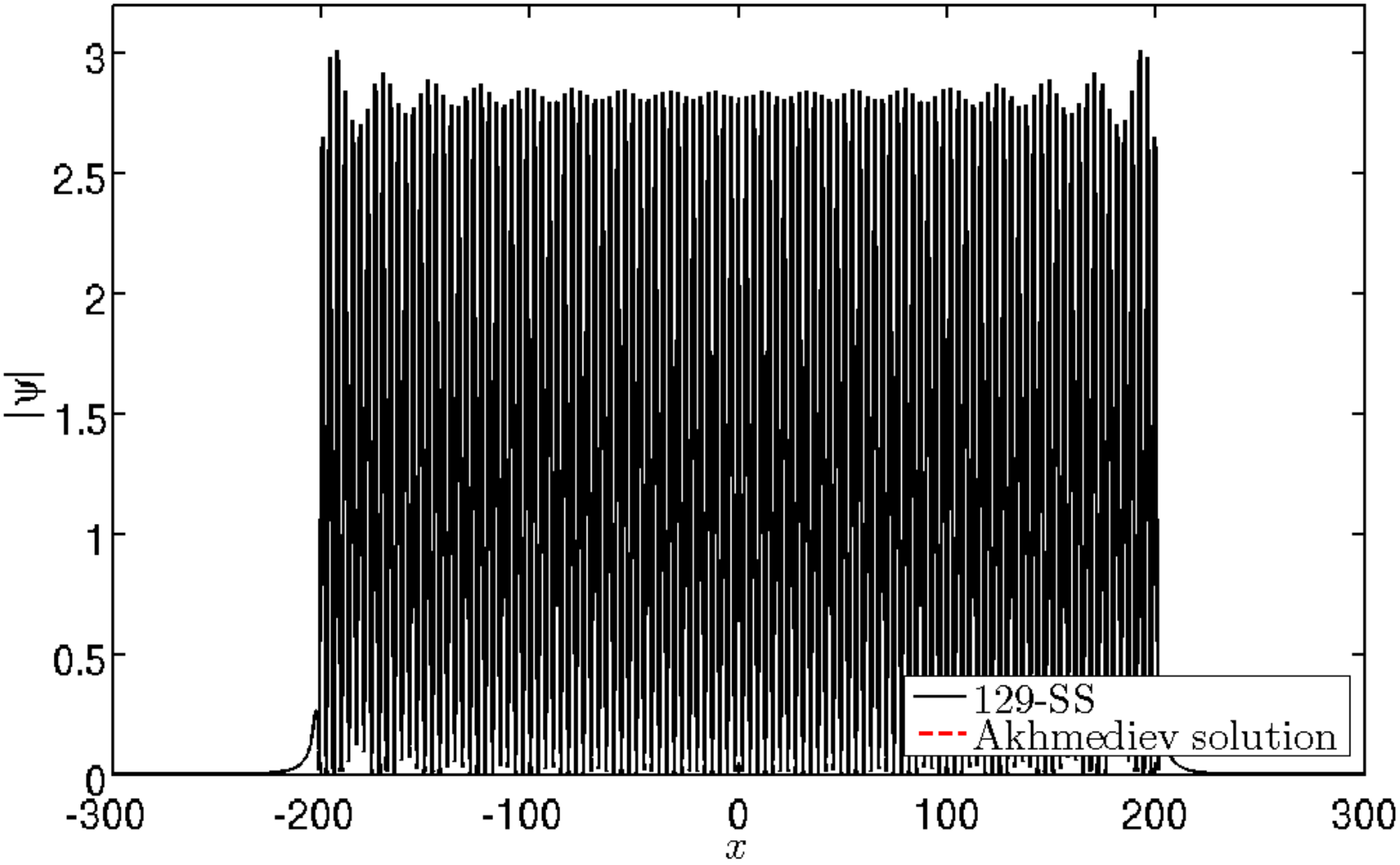

Akhmediev solution modelled with 129-SS: the additional soliton has IST eigenvalue **λ = i*0.5** and phase **θ = π**; all positions are zero.

Thank you for your attention!